Revealing Nanomechanical Deformation at Interface and Degradation in All-Thin-Film Inorganic Electrochromic Device

Journal:	*Nanoscale*
Manuscript ID	NR-ART-10-2022-005558.R1
Article Type:	Paper
Date Submitted by the Author:	27-Dec-2022
Complete List of Authors:	Dong, Dongmei; Florida International University, Electrical and Computer Engineering Lou, Lihua; Florida International University Orikasa Lopez , Kazue ; Florida International University Agarwal, Arvind; Florida International University, Mechanical and Materials Eng. Bhansali, Shekhar; Florida International University,

Revealing Nanomechanical Deformation at Interface and Degradation in All-Thin-Film Inorganic Electrochromic Device

Dongmei Dong [a,*], Lihua Lou [b], Kazue Orikasa Lopez [b], Arvind Agarwal [b], Shekhar Bhansali [a]

[a] Department of Electrical and Computer Engineering, Florida International University, Miami, Florida, USA

[b] Plasma Forming Laboratory, Department of Mechanical and Materials Engineering, Florida International University, Miami, Florida, USA

(*Corresponding author: ddong@fiu.edu)

Abstract

Recent progress in electrochromic (EC) devices has been done in optimizing electrode and device configurations and performance. However, the ion insertion/de-insertion induced charge transfer (CT) nanomechanical effect has remained unexplored, i.e., repetitive electrode size change at the nanoscale and stress/strain generated during electrochemical cycling, which is the focus of this work due to its intimate correlation to the elastic and plastic deformation at the interface. Considering the intervalence electrons, excellent electrochemical kinetics, and dramatic color changes, tungsten oxide (WO_3) and nickel oxide (NiO) films are configurated as the EC cathode and anode materials, respectively, within a full device. Upon extended cycles (>10000), the voids generation and delamination that occurred at the interface account for the performance decay. Encouraged by the findings, nanoindentation mechanical tests and electrical kelvin probe force microscopy are employed to investigate the CT induced effects at the interface. There is a dramatic increase of up to 45% in the elastic young's modulus in colored/charged WO_3 at ~40mC/cm^2. The correlation between CT and synergistic mechanical effect is interpreted by the Lippman equation. Interestingly, despite the charged state (colored; lithiated) with a relatively flat morphology bringing a ~3.4 times higher electrostatic surface potential, the electrical work function unexpectedly decreases, arising from the dominant effect of the dipole layer potential over the chemical potential. The interatomic cohesive energy and equilibrium distance increase bury the seeds for mechanical deformation in the long run. This work provides fundamental insights into electro-chemo mechanics and interdisciplinary concerted interfacial effects at the nano/atomic level. The dependence of surface potential, stress, work function, and cohesive energy on electrochemical kinetics has been interpreted.

Keywords: Nanomechanical effects, electrochromic, charge transfer, work function, surface potential

Introduction

Even though the natural cycle of climate change is an ongoing and unavoidable step of life, history seems to be telling us that when the past civilizations have overstretched themselves or pushed their consumption of natural resources to the brink, the consequence of climate change soon became amplified. We are now in a critical period of time with challenges and opportunities to address climate change by developing environmentally responsible and sustainable energy technologies. Up to 40% of the primary energy loss worldwide is currently in buildings for lighting, heating, ventilation, and air conditioning (HVAC).[1-4] The awareness of being environmentally friendly and carbon dioxide emission issues are driving the rapid development of electrochromic (EC) materials and their associated devices today, especially regarding the implementation of windows or glazing for energy-efficient architectures and buildings.[5] Recently, EC supercapacitors are growing as a promising category of materials in the rising deployment of portable electronics, optoelectronic devices, displays, etc.[6-7] EC energy storage has attracted more and more attention in the recent ten years. In addition to their charge storage applications, they can directly tune the relations between humans and sunlight based on their adjustable and reversible optical properties. It can reduce energy consumption by about 20% in buildings for “smart window glazing” applications.[8-15] The efficient energy storage and derivation enables the green energy cycles and has a broad range of applications in powering lights, LEDs, and portable electronic devices.[16] The visual energy status brings a lot of convenience to modern life. Most renewable energy systems (fuel cells, photovoltaic cells, batteries, solar fuel generators, etc.) have common electrochemical origins, constrained by thermodynamics but further reduced by kinetics. Improving the kinetics imposed by reality relies on the fundamental de-coding at the nano and atomic level with a comprehensive analysis that crosses multiple disciplines.

Despite some EC materials being optimized to reach extended cycling life, the degradation mechanism remains unresolved. A succession of chemical, physical, structural, and mechanical changes in electrochemical energy devices’ charge transfer

(CT) processes are not yet understood at the atomic scale. The further enhanced applications, without any doubt, need a strong fundamental understanding of the underlying mechanisms. Significantly, the EC mechanism and the degradation origin can be understood at the next level. The development of energy storage electrodes for Li-ions insertion devices has been discovered to be limited by the interfacial stability against solid or liquid electrolytes.[17] The interfacial behaviors, stability, and synergistic mechanical changes at the nanoscale and associated electrical variations are largely undiscovered, posing a fundamental challenge for electrochemical CT in the long term.

Most transitional metal oxides show significant synchronous changes in the physical, chemical, optical and mechanical properties upon CT in electrochemical reactions. A model, WO_3, for instance, turns its color from transparent to blue when it is reduced upon Li^+/e^- dual insertion under electrochemical control, and vice visa. In complementary to cathodic WO_3, NiO can be placed at the anode side, switching between brownish and clear states. The mechanical stress/strain induced by the ion insertion/extraction causes significant volumetric expansion/shrinkage, termed "mechanical breathing." Furthermore, the electrode stress/strain is not only a consideration of mechanical stability but also closely associated with electrical charge density and electrochemical potential referred to in the equation from Cannarella:[18,19]

$$\Delta V dq = \sigma \cdot A_C \cdot d\delta$$

Where $d\delta$ represents the cell expansion due to the charge dq. σ is the stress and A_C is the area. ΔV is the voltage increase upon external stress. The additional electrical work ($\Delta V dq$) is done to balance the mechanical work ($\sigma \cdot A_C \cdot d\delta$) to allow the charge to pass through the cell. After repetitive cycles, the "mechanical breathing" will eventually lead to delamination at the interface and the film device degradation. The durability remains a challenge by the underdeveloped interfacial stability of electrode films against the electrolyte layer. The electrode stress status and dynamic evolution remain less recently discovered to date. Imposed by the direct correlation of redox charges, mechanical properties, and stability, it is crucial to conduct investigations to understand the interface and interdisciplinary synergetic effects. To the best of our knowledge, no studies have been focused on the interfacial mechanical origin of the degradation of EC oxide films and devices. It will be of great interest to investigate the effect of ion exchange on the mechanical and other properties at the interface.

This work focuses on CT and the interfacial mechanics in electrochemical redox reactions, which would help understand the degradation of EC materials and other energy materials to design durable multi-layered energy devices. Nanoindentation for nanomechanical and interface characterizations for quantifying interfacial changes is an excellent tool to reveal the origin of the irreversible optical switching and charge capacity losses of EC films and devices. The interdisciplinary electro-chemo-mechanical coupling effect at the nanoelectrode is the main focus of this work. As a further exploration of our previous studies on the degradation mechanism,[20,21] this study focuses on electro-chem-mechanics by deriving young's modulus/hardness evolutions upon Li^+ ions insertion/de-insertion at both anode and cathodic EC pseudocapacitive films. Berkovich-tipped nanoindentation techniques were used to probe the electro-chemo-mechanics of cathodic EC WO_3 and anodic NiO electrodes against the non-aqueous Li^+ electrolyte. The dependence of Young's modulus and hardness on ion insertion/extraction is quantified. The synergetic surface energy and surface electrostatic potential have been investigated, which points to the focused and fundamental questions related to energy storage. The repetitive size change of the electrode materials upon charging (lithiation) and discharging (de-lithiation), termed mechanical breathing, may lead to delamination at the interface upon extended cycles. This work further focuses on the fundamental mechanisms of the degradation regarding the changes in young's modulus, surface potential, work function, and so on based on surface physics, which is critically missing to date, complementing the existing efforts in optimizing the performance and stability of ion-insertion based electrochemical device. The correlation of the fundamental physical changes at the nano/atomic scale on the film surface and interface upon coloration/bleaching and the device degradation after extended cycles point to the unique value of this work and the novelty of the article. The knowledge gained in this study bridges the interdisciplinary electro-chemo-mechanics fundamental research and is beneficial for advancing layered electrochemically ion-insertion energy devices.

Results and discussion

Large optical modulation, long-term durability, and fast response are three key criteria for practical applications of EC devices. The most developed EC devices are configurated with an anode/electrolyte/cathode sandwich-like structure. EC cathodic WO_3 and paired anodic NiO are well known for their excellent color switching and modulation properties based on electrochemical redox reactions under a small voltage bias. It is widely accepted that the ion and electron dual injection/extraction model explains the electrochromism phenomenon. The coloration (or reverse bleaching) is a synchronous electronic and ionic process associated with the intervalence electron transfer under electrochemical control. Here, EC NiO and WO_3 are paired as anodic and cathodic electrodes of the device considering the synchronous coloration under a small positive potential bias and bleaching upon the reverse potential, the comparable charge capacity for lithium and electrons dual injection/extraction; and their combination provides improved color neutrality or hue balance. The device turns colored with the cathode and anode being blue and brownish synchronously, blocking both the visible and near-infrared bands of the solar spectrum (Fig.1a). Upon the reverse bias, the ions and electrons move in the opposite direction, giving rise to the bleached state (Fig.1b). However, long-term durability remains a challenge for the mass adoption of this technology and needs to be overcome. Optical contrast and charge capacity degradation are typically observed after hundreds or thousands of cycles, as discussed in the previous work.[20,21] Here, the charge capacity shrinkage of the device WO_3/Electrolyte(Li^+)/NiO from an initial 40 to degraded 2.5C/cm^2 with potential window from -1.8 to 0.5V (Fig.1d), accompanied by the transmittance modulation $\Delta T\%$ decrease from around 50% to less than 10% over 10,000 cycles (Fig.1d inset). Many efforts have been put into optimizing and investigating single films for improved stability. Still, the interfacial behaviors have been overlooked, which is crucial to the full multilayer device with ions and electrons traveling. In our study, a focused ion beam has employed to look into the interface evolution in the degradation (Fig.1e). After repetitive coloration/bleaching cycles, evident delamination is observed at the interface of the WO_3 and the ion-conducting layer in degradation. It causes the disconnection of the two neighboring layers and immobile the functional Li-ions (Fig.1c). This observation provides a different angle to look into the issues impeding the stability of the EC device and the energy storage supercapacitors and batteries in general.

It can be hypothesized that the accumulation of the mechanical effects is mainly responsible for the eventual failure. We conduct hypothesis-driven mechanical investigations into the cathode and anode coupling electro-chemo-operation to probe the interfacial behavior further.

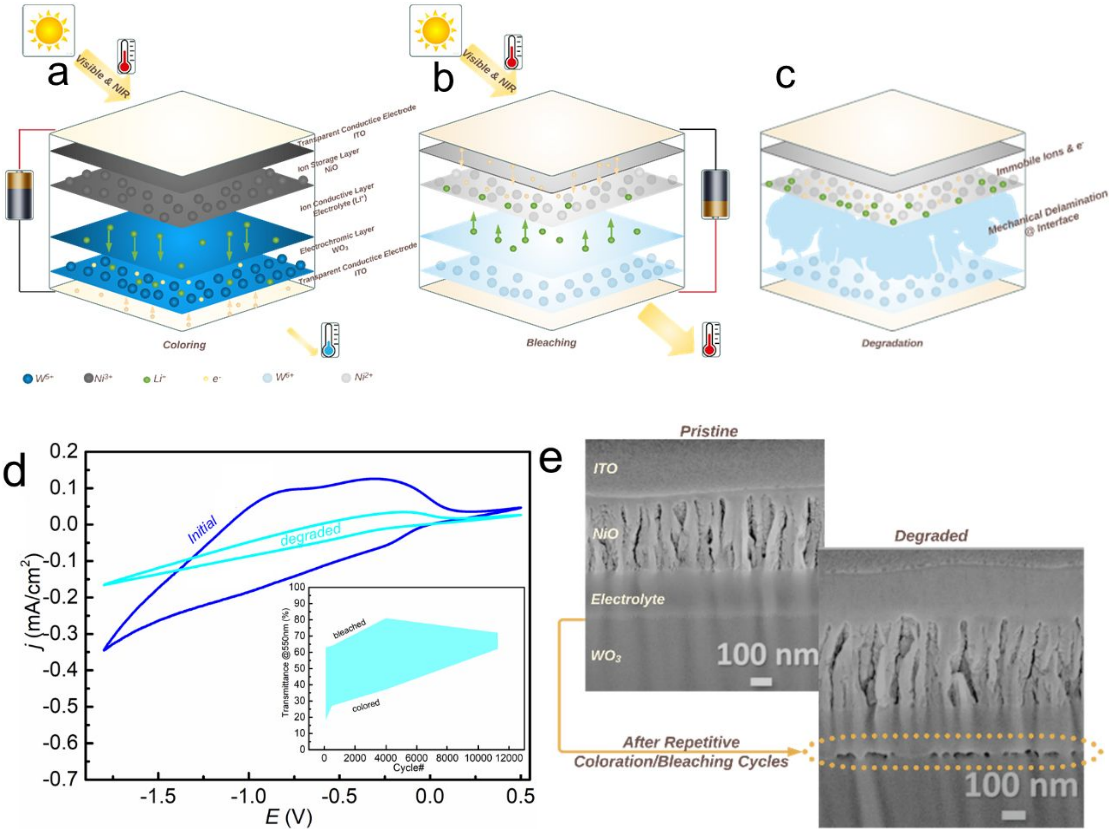

Fig. 1. Unveiling degradation at interface in sandwitch-structure devices. Schematic illustration for the configuration and working mechanism of the ECD during (a) colored and (b) bleaching process for smart window applications. (c) Degraded device diagram proposed. (d) Cyclic voltammograms of initial and degraded ECD upon extended cycles. Inset is the transmittance modulation spectra. (e) Focused ion beam obtained direct evidence of the multi-layered device degradation at the interface.[20]

Encouraged by the findings at the interface, we perform nanoindentation to measure the elastic modulus and hardness of the EC oxide films in the pristine, lithiated, and de-lithiated states for further investigations. The load-displacement response is demonstrated for WO_3 and NiO, respectively (Fig. 2a & 3a). The Young's modulus and hardness variations at colored and bleached states are extracted for both films (Fig. 2b & 3b). The modulus and hardness increase dramatically for colored WO_3 after Li insertion and then decrease for the bleached state after Li extraction. The modulus increases from 87.78 ± 1.43 to 127.5 ± 3.9 GPa, by 45% upon electrons and Li^+ dual injection:

$$WO_3(Transparent) + x(Li^+ + e^-) \leftrightarrows Li_xWO_3(Blue)$$

The modulus bounces back to 112.22 ± 0.7 GPa at the bleached state, followed by reversible oxidation. The redox reactions induced variations in the modulus/hardness as a charging function are summarized (Table 1&2). An electro-chem-mechanical effect is evident from both modulus and hardness values. The yield stress σ_Y can be calculated based on the equation below:[22]

$$\sigma_Y = 0.25 P_{max} c^{-2}$$

It points to the pristine, colored, and bleached stress ratio estimation as 1.46: 2.38: 1. From the initial to lithiation (charged), the stress is increased by 63%. It decreases by 58% from lithiation to the following de-lithiation (discharged). The elastic strain ε can be represented by the equation:

$$\varepsilon = (h_{max} - h_p)/h_{max}$$

The calculated values for the initial, colored, and bleached states are 0.42, 0.4, and 0.34, respectively. The changes in mechanical properties depend on the charge density, charging behavior, and film microstructure. The same procedure determines the elastic modulus and hardness of anodic NiO. However, electrochemical kinetics have a limited effect on its mechanical properties.

An atomic force microscope (AFM) demonstrated the indent's remains after employing the Berkovich tips and morphology upon the Li^+ insertion/de-insertion (Fig. 2c). The AFM images after nanoindentation of the pristine, colored, and bleached states of the same WO_3 film. It is evident that the morphology of the transparent WO_3 film at pristine and bleached states has similar surface morphology, indicating the reversible morphology. After indentation, the colored state revealed a relatively smaller indented area when compared to the initial state (Fig.S2). In comparison, the bleached film gave a much larger indent area associated with a diameter of ~1µm to ~800nm, suggesting that the film becomes harder upon Li insertion due to the redox-induced surface stress.[23] The calculated hardness values (Table 1) are consistent with the cross-section profile analysi

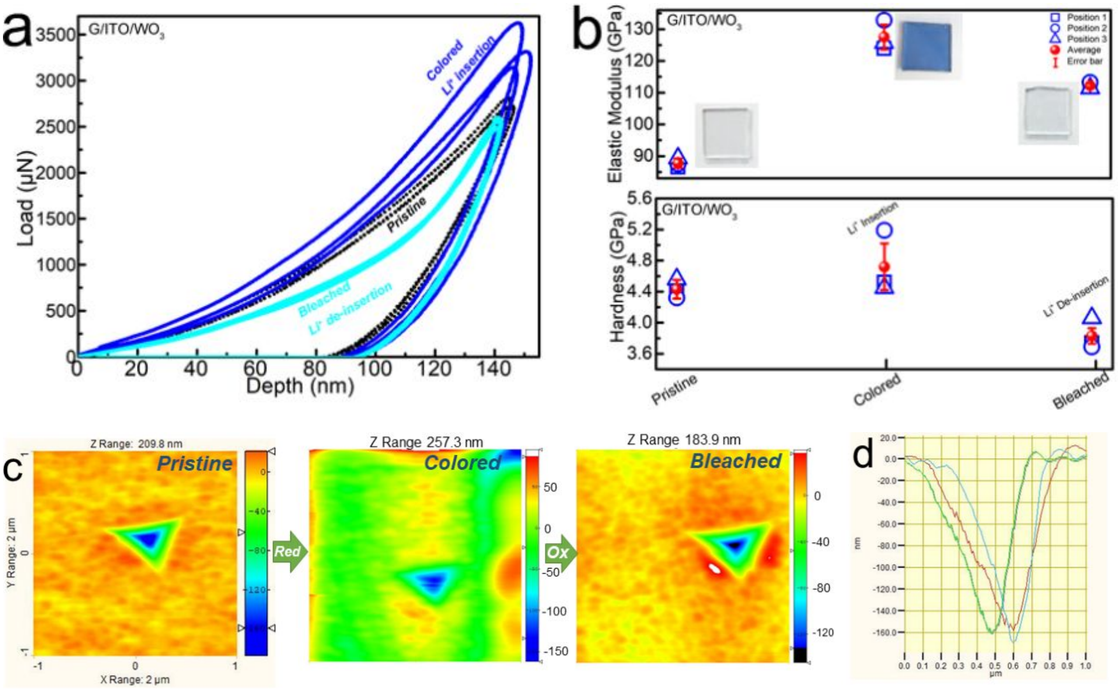

Fig. 2. Nanomechanical investigations of cathodic WO_3 electrode upon redox reactions. (a) Load/unload-displacement curves of nanoindentation tests with a maximum displacement of 150 nm of the pristine, Li^+ inserted (colored), and de-inserted (bleached) states. (b) Evolutions of modulus and hardness upon Li^+ insertion/de-insertion. (c) Topographical images are shown after the nanoindentation of films left by a Berkovich tip. (d) The cross-section profile along with the line of three repetitive nanoindentation measurements of pristine WO_3 film.

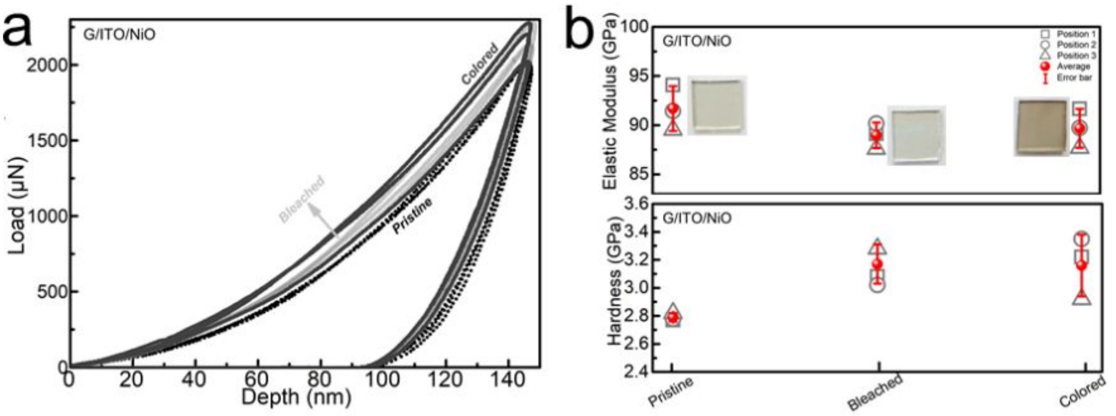

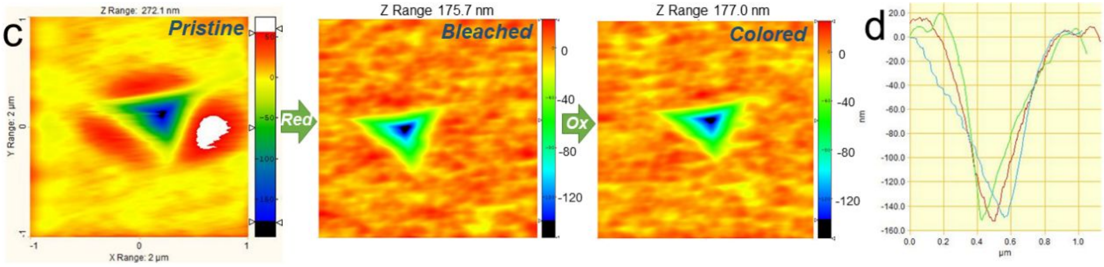

Fig. 3. Nanomechanical investigations of anodic NiO electrode. (a) Load/unload-displacement curves of nanoindentation tests with a maximum displacement of 150 nm of the pristine, bleached, and colored states. (b) Evolutions of modulus and hardness. (c) Topographical images left by a Berkovich tip on the film surface. (d) The cross-section profile along with the line of three repetitive nanoindentation measurements of pristine NiO film.

Table 1 Nanoidentation results of cathodic EC WO_3 films.

Nanoindentation	Step 1 Pristine WO_3	Step 2 Colored WO_3 (Li^+ Insertion)	Step 3 Bleached WO_3 (Li^+ Extraction)
Modulus (GPa)	87.78 ± 1.43	127.5 ± 3.9	112.22 ± 0.7
Hardness (GPa)	4.43 ± 0.12	4.72 ± 0.3	3.67 ± 0.06

Table 2 Nanoidentation results of anodic EC NiO films.

Nanoindentation	Step 1 Pristine NiO	Step 2 Bleached NiO (Li^+ Insertion)	Step 3 Colored NiO (Li^+ Extraction)
Modulus (GPa)	91.69 ± 2.28	88.97 ± 1.30	89.68 ± 1.98
Hardness (GPa)	2.79 ± 0.03	3.17 ± 0.14	3.16 ± 0.22

Young's modulus increase fundamentally originates from the surface charge and the surface free energy.[24] To further understand the electro-chemo stress, we need to revisit the surface free energy, which is represented by surface stress in the Suttleworth equation:[25,26]

$$\sigma = sfe + \frac{\partial sfe}{\partial \varepsilon},$$

Where σ is the surface stress, *sfe* is the surface free energy, and ε is the elastic surface strain. The latter of which is defined as:

$$\partial \varepsilon = \frac{\partial l}{l},$$

Where l is the original length and ∂l refers to the deformation in length.

Surface Properties

To gain a deep insight into the surface properties and surface free energy and understand the surface stress, KPFM is scanned to conduct the surface analysis. A comparison between electrostatic features of the transparent and colored WO_3 films is demonstrated in Fig. 4, which displays the film morphology and the surface potential profiles of a 10 μm section. Notably, the morphology becomes more flattened, and there is a ~78% decrease in the film surface roughness S_a and S_q from the initial to the lithiated coloration state. Considering the profile plot's minimum and maximum voltage values, the initial state shows a lower voltage dynamic range. The incorporated charges at the colored state accompanied by a relatively flat surface bring a ~3.4 times wider variation range of the electrostatic potential on the surface, increasing from -104±11 to 82±13.6mV at the transparent state to -310±68 to 320±59mV in coloration (lithiation). The electrical potential enhancement in the coloration state is an electro-chemo charging effect associated with electronic/ionic movement and dual injection to the electrode WO_3. The electrons and Li^+ ions insertion significantly increases the surface potential and thus decreases the work function based on the equation:[27]

$$W = W_{Tip} - qV,$$

The KPFM tip is coated with PtIr with the work function of 5.4 eV. The average surface potential at the colored state is much higher (lower work function) than that of the initial (larger work function). The lower work function in the bleaching state suggests it is easier to take electrons out of the electrode material compared to the colored state, which is consistent with the faster response time for bleaching in the electrochemical chronoamperometry characterization (Fig.S4). The decrease in the work function will lead to the "e^- repelling" behavior for spontaneous bleaching, which provides fundamental insights into the currently unaddressed memory effect.[28]

The quantitive analysis of the thermodynamic theory describing the properties of the electrode/electrolyte interface is given by the Lippman equation, which connects the electrochemistry and mechanical properties:[29]

$$-\left(\frac{\partial \gamma}{\partial E}\right)_{P,T,\mu_i} = q_M,$$

γ is the interfacial variable conjugate to the surface area as an extensive variable. q_M is the charge density on the electrode side of the interface. E is the electrode potential, and μ_i is the chemical potential of component i. This equation correlates the charge density at interfaces and interfacial tension. The colored WO_3 after multiple-step chronoamperometry test up to -1.0V (v.s. Ag/AgCl) potential, with a charge capacity of ~40mC/cm^2. The strain experimentally obtained for charged WO_3 from the nanoindentation test is at 0.4, agreeing with the theoretical γ value from the Lippman relation.[30]

The electrochemically-induced charge accumulation causes the population of both the electrons and Li$^+$ ions, strengthening the interaction of the molecules and the molecular “spring constant,” which is fundamentally responsible for the mechanical increase in young’s modulus and hardness in the colored state. This strongly reflects the correlation of the electrochemical behaviors and nanomechanical properties of the electrode materials, as well as the determination of electronic/ionic dynamic to macro properties.

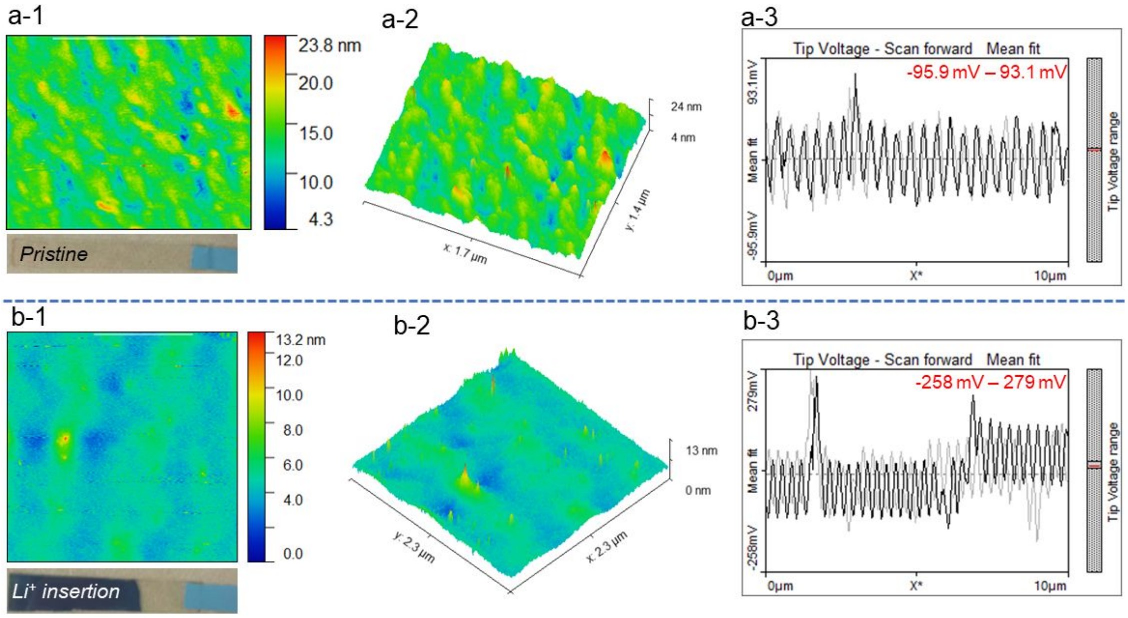

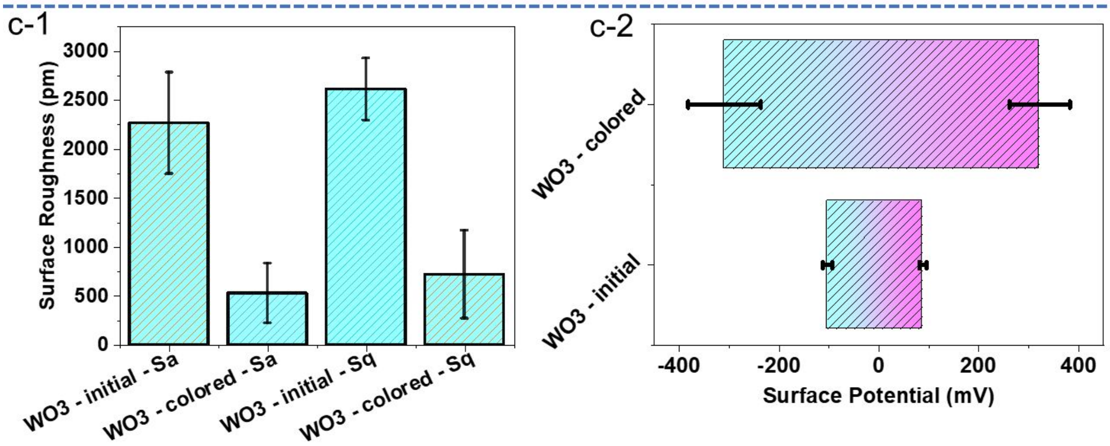

Fig. 4. Morphology analysis by AFM 2D/3D scanning and surface potential by KPFM. WO_3 films in the transparent state (a), colored state (b) at a charge density of ~40mC/cm^2 concerning the surface morphology and electrical potential, and (c) comparison images in roughness and surface potential at both of the two states.

The delamination at the macroscale at the interface originates from the neighboring atoms' distance r increase at the equilibrium state. The KPFM results show an increase in the surface potential, alternatively, cohesive energy, from transparent to colored state (lithiation). Thus, the cohesive curve is expected to move towards the upper right position. Based on the nanoindentation measurement, the young's modulus enhances as well. The cohesive curve with a narrow deeper potential well, higher surface potential, i.e., typically neighboring cohesive energy) and larger equilibrium distance in the colored state is demonstrated in Fig. 5a. After repetitive extended cycles, it is expected that the value of neighboring bonding distance r will exceed the original equilibrium separation r_0, typically cohesive distance, causing the delamination at the interface eventually. Moreover, scientists have been trying to quantitively correlate the young's modules and work functions to investigate the origin of the materials' properties. In recent progress in establishing a generic relation between the young's modulus and the electron work function, the young's modulus is identified as the second-order derivative of interaction potential concerning the equilibrium distance, demonstrating its sextic relation with the work function.[31] Interestingly, there is an abnormal in the artificial materials system with matrix material being the host and Li^+ as guest ions in this work. Despite a significant increase in the young's modulus upon Li^+ insertion, the work function, however, decreases. To fundamentally address it, the chemical potential and the dipole layer potential responsible for the work function at the surface have been proposed. The Li^+ travel from the electrolyte to electrode material leads to a sharp drop even though there is an increase in chemical potential. As demonstrated in Fig.5, the Fermi-level and chemical potential increase at the colored state, but the work function becomes smaller due to the contributions of the much lower dipole layer potential. It indicates the dipole layer potential could be dominant in the work function at the electrode/electrolyte interface, which is definitely in need of more attention and effort in electrochemical kinetics studies.

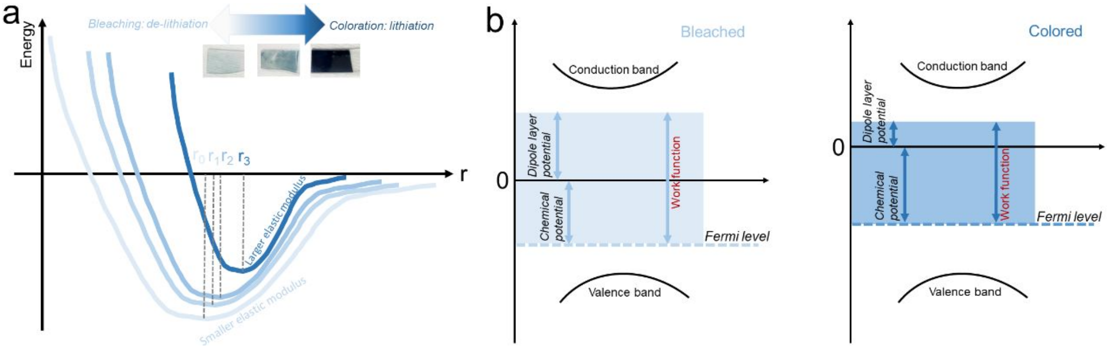

Fig. 5. Physics insight into charge transfer and deformation at the electrochemicl interface. (a) Potential well and equilibrium distance in cohesive curves; (b) The components of the work function: chemical potential and the dipole layer potential.

Pseudocapacitive Charge Storage

No huge variations of modulus and hardness are found in the anodic NiO. The mechanical response arises from different micro features, charge densities, and charge storage mechanisms from WO_3. The electrochemical reaction kinetics for the EC cathodic and anodic electrodes are quantitively studied to elaborate further on the relations of charge storage and corresponding mechanical effect. Firstly, the CV results are analyzed and compared between the two electrodes of the ECD (Fig.6a & b). Pseudocapacitive materials have the electrochemical characteristics of one or a combination of underpotential deposition, surface-redox pseudocapacitance, or bulk-insertion pseudocapacitance.[32] Pseudocapacitive charge storage is faradaic in origin and fundamentally differs from typical electrical double-layer (EDL) materials. As EC electrodes, WO_3 and NiO show a significant difference in the CV curves, and they are also different from typical dark-shape battery materials or rectangular-curve EDL capacitors. For WO_3, as shown by a triangle-like shape with one broad peak, characteristic of typical intercalation pseudocapacitive effects.[33,34] In the case of NiO, two reversible groups of small redox peaks with some separations in the potential appear in the scan. It is a hybrid behavior of EDL (non-faradaic) and ion-diffusion (faradaic) processes. It is acknowledged that the area cycled by the CV curve is representative of the total charges arising from the diffusion and the surface capacitive processes.[35] WO_3 shows a much larger charge capacity than NiO, explaining the more profound electro-chemo coupling mechanical effect. To further analyze the EC pseudocapacitive charge storage mechanism, the surface capacitive effects can be distinguished from the diffusion kinetics employing the power-law $i = av^b$.[36] The capacitive current shown as the shaded area is compared with the total experimental current at the sweep rate of 20 mV/s (Fig.6a & b). The relative contributions of the surface capacitive effects to the total charge storage are also evaluated (Fig.6c). It is obvious that the sub-surface diffusion-controlled kinetics is prominent over the surface behaviors for WO_3 at low scan rates. The charge contribution ratio is about 57% at 30 mV/s. With the scan rate increasing, the diffusion-related portion decreases due to inadequate redox reactions. EIS measurements are performed for cathodic and anodic electrodes at fully colored and bleached states (Fig.6d). Both show a semicircle arc at high-middle frequencies and sharp increased tail-like curves at low frequencies, characteristics of CT resistance, and Warburg impedance with a constant increase of the imaginary and real parts. The NiO shows typical capacitive-like behavior ($\sim 90^\circ$) while WO_3 has a high Warburg impedance ($\sim 45^\circ$) associated with the ion diffusion resistance in the low-frequency f range (Inset of Fig.6d). Notably, the CT resistance is significantly smaller for NiO than WO_3, potentially caused by the difference in the surface redox and challenging bulk-insertion reactions. These comparisons are consistent with the idea that the diffusion-controlled (bulk) pseudocapacitive mechanism in charge storage and synchrony coloration accounts for the WO_3 electrode. In contrast, a dominant surface-limited behavior for NiO (Fig.6e). The limited charge density from surface redox reactions for NiO could account for the smaller variations in the mechanical effect, while the insertion-redox kinetics of WO_3 corresponding to larger charge capacity introduce a stronger mechanical response.

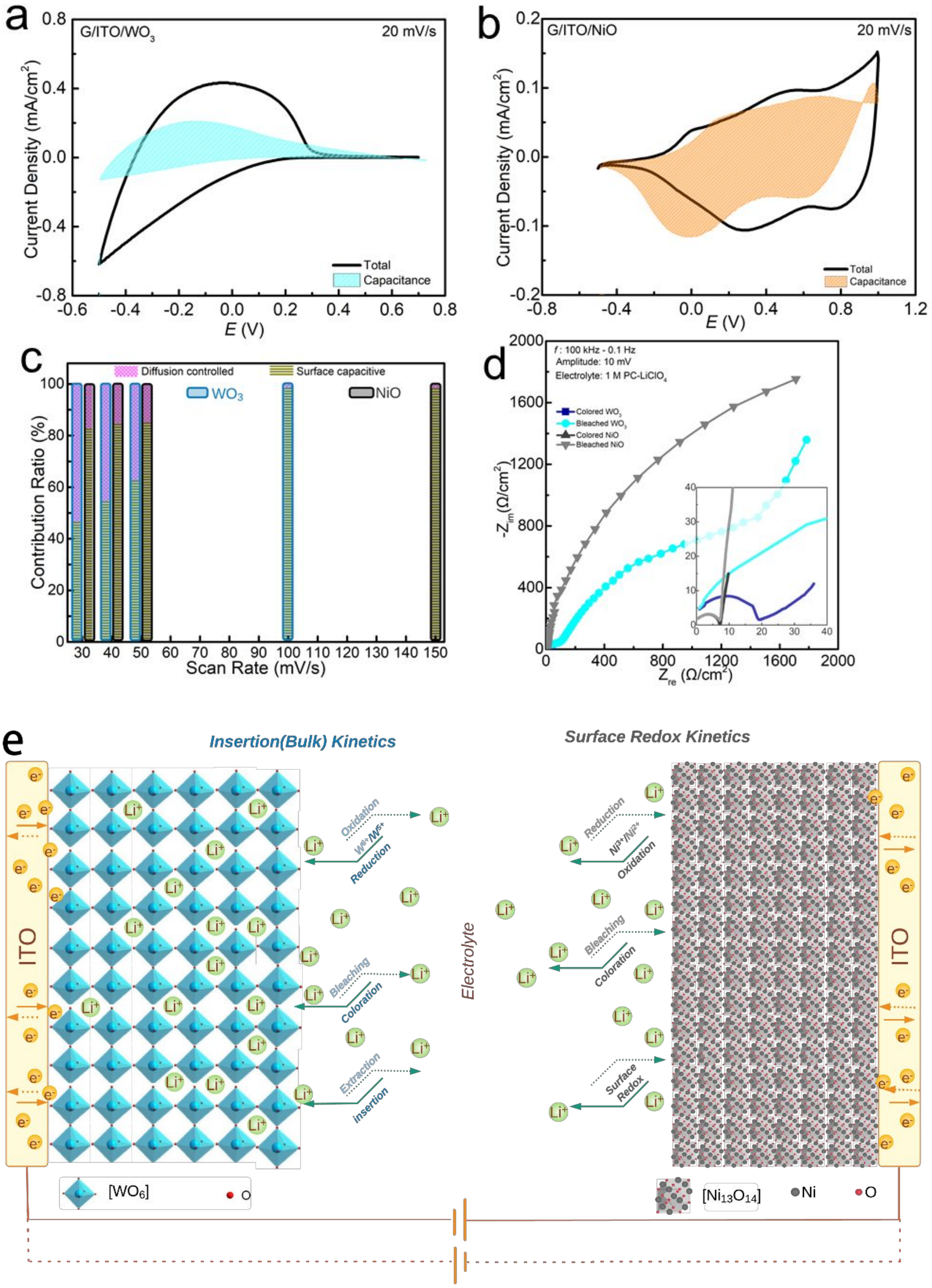

Fig. 6. Electrochemical pseudocapacitive charge storage of the cathodic EC WO_3 and anodic NiO. CV curves at 20 mV/s illustrate the surface capacitance contribution (shadow area) to the total of (a) WO_3 and (b) NiO. (c) Percentage of diffusion-controlled and surface capacitive behavior varying with scan rate. (d) Comparison of

EIS data of WO_3 and NiO. The inset shows the magnified curves in the high-*f* range. (e) ECD's schematic synchronous coloration/bleaching comprises WO_3 Li^+-insertion (bulk) dominant kinetics at the cathode electrode and NiO surface redox dominant at the anode electrode.

Conclusions

Most renewable energy devices share the common electrochemical origin, depending on the thermodynamics, and are further constrained by kinetics. A fundamental understanding of the CT mechanism at the interface and de-coding at the molecular/atomic level is critical for addressing the performance and durability issues from the root. This work attempts to bring out the correlation of ion insertion, nanomechanical stress, termed breathing effect, physical work function, surface potential, and interatomic cohesive energy in the electrochemical CT process in pseudocapacitive EC nanofilms. A significant increase (~45%) in young's modulus is found in the colored WO_3 films upon lithiation (~40mC/cm^2). The charge accumulation is accompanied by the rise in the surface potential (~3.4 times higher). Based on the KPFM results, there is a decrease in the physical work function in coloration, which is unexpected according to the young's modulus increase. It is proposed this abnormally arises from the much lower dipole layer potential on the surface upon dual Li^+/e^- insertion in coloration. The increased atomic neighboring bonding energy and equilibrium distance will lead to mechanical delamination at the interface after extended cycles, limiting the macro-level performance and durability of most of the renewable electrochemical systems.

Experimental

Electrochromic oxides films and device fabrication

The WO_3 and NiO films were deposited on Glass/ITO substrates with direct current magnetron sputtering techniques. The sputtering parameters of the films and thickness were described in previous work.[18,19] The lithium perchlorate $LiClO_4$ powder (purity: 99^+%, Thermo Scientific) and propylene carbonate (PC) liquid (purity: 99.5%, Thermo Scientific) were mixed to prepare the electrolyte 1M $LiClO_4$-PC.

Electrochromic and electrochemical characterizations

Using Pt wire as the counter electrode and Ag/AgCl as the reference electrode, the electrochemical test and Li^+ insertion/extraction from 1M $LiClO_4$-PC electrolyte to EC film electrodes were carried out at AutoLab (Metroohm, PGSTAT30 potentiostat) workstation. Cyclic voltammetry (CV), chronoamperometry (CA), and electrochemical impedance spectroscopy (EIS) were performed with a three-electrode configuration for single films. For the electrochemical characterization of EC devices, the reference electrode is connected to the counter electrode side. The UV-Vis spectrometer recorded the optical transmission spectra as a function of cycle number or applied potential.

Nanomechanical measurement

Nanoindentation was carried out using a Tribo-Indenter system (Hysitron Inc., Ti-900) equipped with a standard diamond Berkovich tip. The measurements were taken with the loading and unloading procedures under Quasi-Static nanoindentation. Atomic force microscopy built in the nanoindentation system was employed to record the indentation imprint. We have performed nanoindentation to measure the elastic modulus and hardness of both the anodic and cathodic EC films in the initial, colored, and bleached states using a Hysitron® Triboindenter Ti-900 with a probe geometry of Berkovich. A total of three locations were indented and imaged for each state for both cathodic WO_3 and anodic NiO. Calibration has been performed prior to the quasi-static nanoindentation. The tests were carried out with displacement control mode with a maximum displacement of 150nm. The loading function includes loading and unloading segments of 10s, respectively. The data analysis was done with the Oliver-Pharr analytical model and TriboScan analysis software. The mechanical properties, including reduced elastic modulus and hardness, were obtained. The topographic 2D/3D images were acquired over 2μm × 2μm with scanning probe microscopy and scanning probe image processor software.

KPFM surface potential and theory

To investigate the nanoscale surface potential of EC films, kelvin probe force microscopy (KPFM) has been carried out with the FlexAFM system of Nanosurf (Liestal, Switzerland). The conductive electrical probe was purchased from

Nanosensors (Santa Clara, CA). The cantilever parameters are 75 kHz of frequency, 2.8 N/m of spring constant, and 225 μm of length. The PtIr5 coating is an approximately 25 nm thick double layer of chromium and platinum iridium5 on both sides of the AFM cantilever. Using KPFM, images were recorded with local contact surface electrical charges, which are the potential differences between the conductive probe and EC films

Conflict of interest

The authors declare no conflict of interest

Acknowledgments

Department of Energy (DoE), US - M2FCT supports this work under award AWD000000013872 (LBNL No. 7621351). DoE - NNSA also supports this work funded under the minority-serving institutional partnership program (MSIPP) ASTERIX consortium under award NA0003981.

References

1. M. Sathiy, A. S. Prakash, K. Ramesha, J. M. Tarascon, and A. K. Shukla, *J. Am. Chem. Soc.*, **133**, 16291 (2011).
2. T. M. Dinh, A. Achour, S. Vizireanu, G. Dinescu, L.Nistor, K. Armstrong, D. Guay, and D. Pech, *Nano Energy*, **10**, 288 (2014).
3. Q. Wei, R. H. DeBlock, D. M. Butts, C. Choi, and B. Dunn, *Energy Environ. Mater.*, **3**, 221 (2020).
4. B. G. Priyadarshini, S. Aich, M. Chakraborty, *Thin Solid Films,* **616**, 733 (2016).
5. S. Zhang, S. Cao, T. Zhang, A. Fisher, J. Y. Lee, *Energy Environ. Sci.* **11**(10), 2884 (2018).
6. S. Mondal, Y. Ninomiya, M. Higuchi, *ACS Appli. Energy Mater.* **3**(11), 10653 (2020).
7. S Mondal, D. Chandra Santra, Y. Ninomiya, T. Yoshida, M Higuchi, ACS Appli Mater. Interface **12**(52), 58277 (2020).
8. C. J. Barile, D. J. Slotcavage, J. Hou, M. T. Strand, T. S. Hernandez, M. D. McGehee, *Joule*, **1**, 133 (2017).
9. R. T. Wen, C. G. Granqvist, G. A. Niklasson, *Nat. Mater.*, **14**, 996 (2015).
10. X. Liang, S. Guo, M. Chen, C. Li, Q. Wang, C. Zou, C. Zhang, L. Zhang, S. Guo, H. Yang, *Mater. Horiz.*, **4**, 878 (2017).
11. H Lin, L. Yang, X. Jiang, G. Li, T. Zhang, Q. Yao, G. W. Zheng, J. Y. Lee, *Energy Environ. Sci.*, **10**(6), 1476 (2017).
12. X. Yang, G. Zhu, S. Wang, R. Zhang, L. Lin, W. Wu, Z. L. Wang, *Energy & Environ. Sci.*, **5**, 9462 (2012).
13. P. Yang, P. Sun, Z. Chai, L. Huang, X. Cai, S. Tan, J. Song, W. Mai, *Angew. Chem. Int. Ed. Engl.*, **53**, 11935 (2014).
14. X. Xia, Z. Ku, D. Zhou, Y. Zhong, Y. Zhang, Y. Wang, M. J. Huang, J. Tu, H. J. Fan, *Mater. Horiz.*, **3**, 588 (2016).
15. L. Liu, K. Du, Z. He, T. Wang, X. Zhong, T. Ma, J. Yang, Y. He, G. Dong, S. Wang, X. Diao, *Nano Energy*, **62**, 46 (2019).
16. W. Y. Tsai, R. Wang, S. Boyd, V. Augustyn, N. Balke, *Nano Energy*, **81**,105592 (2021).

17. J. Cannarella, C. Z. Leng, C. B. Arnold, On the coupling between stress and voltage in lithium-ion pouch cells. Energy Harvesting and Storage: Materials, Devices, and Applications V, *SPIE*, **9115**, 69 (2014).
18. M. Lei, B. Xu, Y. Pei, H. Lu, Y. Q. Fu, *Soft Matter*, **12**(1), 106 (2016).
19. F. Tian, J. H. Pei, D. L. Hedden, G. M. Brown, T. Thundat, *Ultramicroscopy*, **100**(3-4), 217 (2004).
20. D. Dong, W. Wang, A. Rougier, G. Dong, M. Da Rocha, L. Presmanes, K. Zrikem, G. Song, X. Diao, A. Barnabé, *Nanoscale*, **10**(35):16521 (2018).
21. D. Dong, W. Wang, A. Rougier, A. Barnabé, G. Dong, F. Zhang, X. Diao, *J. Mater. Chem. C*, **6**(37), 9875 (2018).
22. R. Suttleworth, *Proc. Phys. Soc. London A,* **63**, 444 (1950).
23. R. Raiteri, H.-J. Butt, M. Grattarola, *Electrochim. Acta,* **46**, 157 (2000).
24. Y. Zhang, J. Zuo, Y. Gao, P. Li, W. He, Z. Zheng, *J. Phys. Chem. Solids*, **131**, 27 (2019).
25. G. G. Láng, *J. Solid State Electrochem.* **24**(11), 3039 (2020).
26. T. S. Mathis, N. Kurra, X. Wang, D. Pinto, P. Simon, Y. Gogotsi, *Adv. Energy Mater.*, **9**(39), 1902007 (2019).
27. L. Liu, Q. Zhang, K. Du, Z. He, T. Wang, Y. Yi, M. Wang, X. Zhong, G. Dong, X. Diao, *J. Mater. Chem. A.*, **7**(40), 23028 (2019).
28. Y. Shi, M. Sun, Y. Zhang, J. Cui, X. Shu, Y. Wang, Y. Qin, J. Liu, H. H. Tan, Y. Wu, *ACS Appl. Mater. Interface*, **12**(29), 32658 (2020).
29. E. I. Ismatove, B. O.Sarsenbaev, Lippman-schwinger equation solution for diffraction interaction charge particles (2008).
30. G. Hua, D. Li, *Appl. Phys. Lett.*, **99**(4), 041907 (2011).
31. S. Zhang, S. Cao, T. Zhang, A. Fisher, J. Y. Lee, *Energy Environ. Sci.*, **11**(10), 2884 (2018).
32. Y. Wang, E. L. Runnerstrom, D. J. Milliron, *Annu. Rev. Chem. Biomol. Eng.,* **7**, 283 (2016).
33. C. G. Granqvist, M. A. Arvizu, İ. Bayrak Pehlivan, H. Y. Qu, R.T. Wen, G. A. Niklasson, *Electrochim. Acta*, **259**, 1170 (2018).
34. G. Cai, A. L.-S. Eh, L. Ji and P. S. Lee, *Adv. Sustainable Syst.*, **1700074** (2017).
35. Y. Ke, J. Chen, G. Lin, S. Wang, Y. Zhou, J. Yin, P. S. Lee, Y. Long, *Adv. Energy Mater.* **9**(39), 1902066 (2019).
36. Y. Xiao, Y. Wang, S. H. Bo, J. C. Kim, L. J. Miara, G. Ceder, *Nature Rev. Mater.,* **5**(2), 105 (2020).